Structural and physicochemical insights into pH-responsive poly(DEAEMA-*co*-HEMA)-grafted mesoporous silica nanoparticles

Lorena García-Uriostegui[1*], Shuo Qian[2], Gergely Nagy[2], Gregorio Guadalupe Carbajal-Arizaga[3], H. Iván Meléndez-Ortiz[4]

[1]SECIHTI-Centro Universitario de Ciencias Exactas e Ingenierías, Universidad de Guadalajara, Blvd. Gral. Marcelino García Barragán 1421, Olímpica, 44430 Guadalajara, Jalisco, México.
[2]Neutron Scattering Division, Oak Ridge National Laboratory, Oak Ridge, Tennessee 37831, United States.
[3]Departamento de Química, Universidad de Guadalajara, Blvd. Gral. Marcelino García Barragán 1421, Olímpica, 44430 Guadalajara, Jalisco, México.
[4]SECIHTI-Centro de Investigación en Química Aplicada, Blvd. Enrique Reyna Hermosillo #140, 25294 Saltillo, Coah., México.

*Corresponding author: L. García-Uriostegui
lgarciaur@secihti.mx; lorena.garcia39@academicos.udg.mx

Abstract

Mesoporous silica nanoparticles (SiO_2) grafted with responsive polymer shells are versatile hybrid systems. Understanding their three-dimensional organization in the hydrated state remains a significant challenge. Here, SiO_2 nanoparticles were functionalized with a poly(DEAEMA-*co*-HEMA) shell via a "grafting-from" polymerization strategy in aqueous media. Successful surface modification was confirmed by FTIR, thermogravimetric analysis, transmission electron microscopy, X-ray photoelectron spectroscopy, N_2 sorption, and ζ-potential, yielding grafting contents of 22% ($p1_{\mathbf{DEAEMA\text{-}co\text{-}HEMA}}$) and 49% ($p2_{\mathbf{DEAEMA\text{-}co\text{-}HEMA}}$).

Small-angle neutron scattering (SANS) with solvent contrast variation was employed to elucidate the solution-state core–shell architecture of p1 and p2 hybrids at pH 2, where the grafted polymer shell is protonated and highly hydrated. Near contrast matching of the silica core, theoretically estimated at 58% D_2O, suppressed the scattering intensity, enhancing sensitivity to the polymer shell. Constrained core–shell ellipsoid modeling across solvent contrasts revealed a systematic increase in shell thickness, overall particle dimensions, and shell anisotropy with increasing grafting content. In solution, the hydrated polymer shells were markedly more extended and structurally anisotropic than suggested by dry-state techniques structural characterization, highlighting the importance of solution-state structural analysis for accurately describing grafted polymer architectures.

Keywords: pH-responsive polymers; core-shell biomaterials; mesoporous silica nanoparticles; small-angle neutron scattering (SANS); grafting-from polymerization; surface functionalization.

Introduction

The advancement of drug delivery systems critically relies on materials that offer tailored structural versatility, physicochemical tunability, and inherent biocompatibility. Mesoporous silica nanoparticles (MSNs) have emerged as preeminent candidates due to their tunable pore structure, high surface area, and facile surface modification, which make them ideal for the encapsulation and targeted delivery of therapeutics [1, 2]. This approach is particularly transformative in cancer therapy, where enhancing efficacy and minimizing systemic toxicity hinges on precise delivery [3]. To achieve active targeting and controlled release, significant effort has been directed toward the development of hybrid nanomaterials formed by functionalizing MSNs with stimuli-responsive polymers [4]. Grafting stimuli-responsive polymers such as poly(2-(diethylamino)ethyl methacrylate)(PDEAEMA), onto the mesoporous silica surface enables the creation of nanostructures sensitive to physiologically relevant pH or temperature variations [5-8]. The PDEAEMA with a pKa ~ 6.7 [9], functions as a crucial pH-responsive switch due to the protonation of its tertiary amino groups in acidic environments. This characteristic provides an ideal opportunity for pH-controlled drug release [10-14]. Therapeutic efficacy is enhanced by exploiting the pH gradient between healthy tissue (~7.4) and tumor microenvironment (~6.5 – 6.8), as well as the progressive acidity within intracellular compartments (endosomes ~5.5 – 6.0 and lysosomes ~4.5 – 5.0), which provides an internal stimulus capable of triggering sequential drug release and enhancing therapeutic response. For instance, Beagan et al [10]. developed folic-acid-terminated PDEAEMA brush-gated magnetic MSNs, achieving enhanced doxorubicin release under acidic conditions relevant to tumor environments. More recently, a related MSN–PDEAEMA-based nanoplatform incorporating PEG-derived outer layers demonstrated minimal cargo leakage at physiological pH and significantly accelerated release under acidic conditions, while maintaining excellent cytocompatibility [15]. These systems clearly highlight the role of PDEAEMA as an efficient pH-sensitive gatekeeper for controlled intracellular drug delivery.

Furthermore, the incorporation of 2-hydroxyethyl methacrylate (HEMA) as a comonomer provides an additional level of control over the physicochemical properties of the polymer shell. Poly(HEMA) is well known for its high hydrophilicity, excellent biocompatibility, and resistance to nonspecific protein adsorption, properties that are highly desirable in biomedical nanocarriers [7, 16]. When combined with pH-responsive PDEAEMA, the resulting HEMA-*co*-DEAEMA copolymer enables simultaneous modulation of hydration, chain conformation, and interfacial interactions, offering a versatile platform to fine-tune shell structure and responsiveness. However, systematic studies evaluating how polymer grafting content influences the three-dimensional core–shell architecture, shell uniformity, and structural integrity of MSN-based hybrids, particularly in the hydrated state, remain scarce. Moreover, while analogous systems based on DEAEMA are widely reported, the combined effects of the bulkier diethylamino group in DEAEMA and the hydrophilic HEMA comonomer on shell conformation, coverage, and responsiveness have not been thoroughly explored.

While small-angle neutron scattering (SANS) has been extensively applied to polymer–grafted silica systems assuming perfectly spherical cores and uniform shells [17-20], significantly less is known about

how core anisotropy, grafting-from synthesis, and copolymer composition combine to produce heterogeneous shell architectures. Understanding these non-ideal, direction-dependent structures in the hydrated state is critical for accurately predicting and controlling molecular transport in stimuli-responsive nanocarriers. To address these gaps, the present work aims to synthesize and investigate hybrid nanomaterials based on mesoporous silica nanoparticles grafted with DEAEMA-*co*-HEMA copolymeric shell at controlled grafting levels using a grafting-from polymerization strategy. This approach enables polymer chains to grow directly from surface-anchored initiators, providing distinct advantages such as high grafting quantity, precise control over the polymer shell thickness, and enhanced colloidal stability [21, 22]. Consequently, these features enable the creation of complex architectures while accounting for spatial variations in chain length and local surface coverage. The study is designed to evaluate how polymer composition, grafting amount, and grafting conditions influence the structural organization and interfacial properties of the resulting core–shell systems

Although conventional transmission and scanning electron microscopy (TEM and SEM) provide valuable information on particle morphology, and a proportional relationship with the grafting polymer length[23-26], they are inherently limited in capturing the true three-dimensional architecture of polymer grafted core–shell systems in the hydrated state, where biological functionality is defined. TEM effectively resolves the silica core but often struggles to distinguish the polymeric shell due to its low electron density contrast. Dynamic light scattering (DLS) offers rapid estimation of hydrodynamic size and colloidal stability; however, it lacks the ability to resolve internal structural features or shell thickness and typically assumes idealized spherical geometries, potentially obscuring anisotropies induced by the silica core morphology [25]. Therefore, small angle neutron scattering (SANS) was employed as a complementary technique to obtain statistically representative structural information in solution, enabling the determination of particle shape, shell thickness, and polymer density distribution through contrast variation methods, as widely demonstrated for polymer-grafted and core–shell nanostructures [20, 27, 28].

In the end, this work seeks to establish a robust structure–property relationship for SiO_2-g-poly(HEMA-co-DEAEMA) systems and to demonstrate how controlled copolymer grafting via a grafting–from polymerization governs the hydrated shell architecture relevant to stimuli-responsive nanocarriers. By combining advanced scattering techniques with comprehensive physicochemical characterization, this study highlights the importance of solution-state structural analysis for the rational design of next-generation intelligent drug delivery platforms.

2. Materials and methods

2.1 Materials

Tetraethylorthosilicate (TEOS, 99%), vinyltrimethoxysilane (98%), *N*-cetyltrimethylammonium bromide (CTAB, 98%), 2,2'-Azobis(2-methylpropionitrile) (AIBN, 99%), N,N'-Methylenebis(acrylamide) (NMBA, 99%) anhydrous toluene (99.8%), 2-(Diethylamino) ethyl methacrylate (DEAEMA, 99%), phosphate buffered saline (PBS 10 mM, pH 7.4) were from Sigma-Aldrich (Toluca, Mexico) and used as received.

Ethanol (97%), sodium hydroxide (NaOH, 97%) and sodium chloride (NaCl, 97%) were purchased from Analytyka de Mexico SA de CV. Ultrapure water (Milli-Q, 18.2 MΩ·cm) and deionized water (Selectropura, Mexico). 2-Hydroxyethyl methacrylate (HEMA, 97%), from Sigma-Aldrich (Toluca, Mexico), was purified by vacuum distillation.

2.2 Synthesis and functionalization of mesoporous silica nanoparticles (SiO_2) with vinyl groups

SiO_2 nanoparticles were prepared by a base-catalyzed sol-gel procedure. Briefly, 3.5 mL of NaOH solution (2 M) was mixed with 480 mL of distilled water and the temperature was raised to 80 °C. Then, CTAB (1 g) was added to the solution under magnetic stirring. After the solution turned clear, 5 mL of TEOS were dropped slowly. The mixture was stirred for 2 h at 80 °C and the product was filtered, rinsed several times with deionized water and ethanol, dried at room temperature, and finally calcined under air atmosphere at 550 °C for 4 h (heating rate of 1 °C min^{-1}) [29, 30].

To provide vinyl groups to SiO_2, vinyltrimethoxysilane (VSyl) was grafted onto the surface by a condensation method. Briefly, 100 mg of silica particles were dried (overnight in vacuum at 60 °C) and then dispersed in 25 mL of dry toluene, heated to 80 °C under stirring, and nitrogen-degassed for 30 minutes. Then, 0.300 mL VSyl was added, the reaction was stirred at 110 °C under N_2 for 24 h. The SiO2/VSyl product was ethanol-washed and vacuum-dried in the room temperature.

2.3 Synthesis of the core-shell SiO_2-g-poly(HEMA-*co*-DEAEMA)

The preparation of the hybrid core-shell system was carried out by radical polymerization. First, 50 mg of SiO_2/VSyl was dispersed in an aqueous monomer solution. These solutions were prepared at 3 and 4.5% w/v monomers concentrations. A (SiO_2/VSyl)-to-comonomer mass ratio of 1:3 and 1:4.5 (w/w) was used, respectively. The DEAEMA:HEMA mass ratio was fixed at 80:20 (w/w). Subsequently, AIBN and NMBA were added at 5 and 1% w/w (relative to the comonomers), respectively. Table 1 summarizes the specific quantities of each component. The hybrid materials, SiO_2-g-p(HEMA-co-DEAEMA were labelled as **$p1_{DEAEMA\text{-}co\text{-}HEMA}$** for 3% and **$p2_{DEAEMA\text{-}co\text{-}HEMA}$** for 4.5% monomers concentrations.

The mixture was sonicated for 20 min to ensure homogeneity, and N_2-degassed for 20 min. The polymerization reaction was conducted at 70 °C for 24 h. Finally, the resulting materials were washed several times with deionized water and ethanol to remove unreacted components and dried at 70 °C for 24 h.

Table 1. Experimental formulation for the preparation of $p1_{DEAEMA\text{-}co\text{-}HEMA}$ and $p2_{DEAEMA\text{-}co\text{-}HEMA}$ hybrids

ID	SiO_2/VSyl (mg)	H_2O (mL)	DEAEMA (mg)	HEMA (mg)	NMBA (mg)
$p1_{DEAEMA\text{-}co\text{-}HEMA}$	50	5	120	30	1.5
$P2_{DEAEMA\text{-}co\text{-}HEMA}$	50	5	180	45	2.25

2.4 Structural characterization.

2.4.1 Attenuated total reflectance integrated Fourier transform infrared (ATR - FTIR) spectroscopy

The ATR-FTIR spectra were carried out using a Perkin-Elmer Spectrum 100 spectrometer with a diamond tip (Perkin Elmer Cetus Instruments, Norwalk CT), in the frequency range of 4000 – 650 cm^{-1} over 32 scans. All samples were measured as dried powders at room temperature.

2.4.2 Thermogravimetric analysis (TGA)

The TGA was performed from 25 to 750 °C on a TGA-Q50 (TA Instruments, New Castle, DE) at a heating rate of 10 °C/min under a constant flow of 25 mL/min N_2 atmosphere. Polymer grafted mass percentage and fraction (ϕ) was calculated using the mass loss from 200 to 750 °C (to ensure that the solvent was excluded) after subtracting the mass loss that was recorded for unmodified silica over this temperature range.

The calculation of the dry polymeric shell thickness (***t***) was determined according to the relationship for core-shell particles based on gravimetric measurements [Equation 1] [31]. Due to the ellipsoidal morphology of the SiO_2 core, the effective sphere radius (r_{eff}) was first determined using Equation [2]. Details regarding the calculation method and core dimensions ($r_{\_eq}$ and $r_{\_polar}$) are provided in the supplementary material (SM1.1).

$$\boldsymbol{t = r_{eff}\left[\sqrt[3]{\frac{\phi(\rho_{core}-\rho_{shell})+\rho_{shell}}{\rho_{shell}(1-\phi)}} - 1\right]} \qquad \textbf{[1]}$$

$$\boldsymbol{r_{eff} = \sqrt[3]{(r_{eq})^2(r_{polar})}} \qquad \textbf{[2]}$$

Where:

- $\boldsymbol{\varphi}$ is the polymeric shell mass fraction.
- $\boldsymbol{r_{\_eq}}$ and $\boldsymbol{r_{\_polar}}$ are the equatorial and polar radii of SiO_2 core.
- $\boldsymbol{\rho_{core}}$ (2.2 g/cm^3) and $\boldsymbol{\rho_{shell}}$ (1.15 g/cm^3) are densities of the core and polymeric shell, respectively.

2.4.3 Transmittance electronic microscopy

The morphology of the silica core and core-shell system was examined by transmission electron microscopy (TEM). The analysis was performed on a JEOL JEM-1010 instrument (JEOL Ltd., Tokyo, Japan) operating at 80 kV. Samples were prepared by sonicating the nanoparticles in deionized water and depositing the suspension onto a carbon-coated copper grid.

For quantitative TEM analysis, particle dimensions were extracted from two-dimensional micrographs using ImageJ software [32]. Approximately 80 individual silica cores were analyzed to determine size and shape parameters, ensuring a statistically representative sample.

2.4.4 Nitrogen sorption analysis

The textural properties of samples were determined by nitrogen sorption isothermal studies by using a Horiba BET surface area analyzer (SA-9600) at -196 ◦C. Before measurements, the samples were degassed under vacuum at 120 °C overnight. BET (Brunauer–Emmet–Teller) specific surface area values were determined from the sorption data in P/P_0 relative pressure range from 0.049 to 0.285. The total pore volume (V_P) was calculated based on the adsorption amount at P/P_0 of 0.92.

2.4.5 X-ray photoelectron spectroscopy (XPS)

The XPS studies were carried out using a Phoibos 150 spectrometer with a one-dimensional detector 1D-DLD (SPECS, Germany) and XR 50 M monochromatic AlKα radiation source ($h\nu$=1486.6 eV). Samples were mounted on a steel sample holder for elemental analysis. The elemental composition in atomic percentage (% at.) and the chemical environment of the elements in the samples were obtained by XPS analyses (survey- and high-resolution spectra). Survey spectra were acquired at a pass energy of 40 eV, a dwell time of 0.1s, and energy steps of 0.5 eV. The high-resolution spectra were measured at 15 eV pass energy with step 0.1 eV, dwell time 0.1 s and 15 repetitions. The elemental composition and chemical states were determined from the high-resolution spectra using AAnalyzer software, which is freely available at https://xpsoasis.org/ [33]. The peak fitting procedure employed a Shirley-type background subtraction and mixed Gaussian-Lorentzian line shapes. Atomic percentages were calculated by integrating the peak areas and correcting them using standard Scofield sensitivity factors.

2.4.6 Electrophoretic mobility

The ζ -Potential was determined using a Nano-ZS90 (Malvern Instruments Ltd, Worcenstershire, UK), equipped with a 4-mW helium-neon laser operating at a wavelength of 633 nm and utilizing a fixed scattering angle of 90 degrees. Samples were prepared by dispersing them at a concentration of 2 mg mL^{-1} in PBS. The pH of the PBS buffer solutions was adjusted to 2, 4, 6, and 8 using either 1 M hydrochloric acid (HCl) or 1 M sodium hydroxide (NaOH) as appropriate.

2.4.7 Small Angle Neutron Scattering (SANS)

The SANS experiments were conducted using the extended Q-Range small-angle neutron scattering diffractometer (EQ-SANS) at the Spallation Neutron Source (SNS, beamline BL-6) at Oak Ridge National Laboratory (ORNL, USA) [34]. Measurements were performed in quartz cuvettes of path length of 1 mm using a temperature-controlled sample holder. All SANS measurements were performed in PBS pH 2 to ensure full protonation of DEAEMA units and maximize the contrast of the polymer shell. The SLD of the copolymer shell was estimated for each PBS-H_2O/D_2O mixture accounting for H/D exchange at the protonatable DEAEMA nitrogen (Table SM2, Supplementary Material). These values provided sufficient contrast against the SiO_2 core across all solvent compositions.

To cover a wide scattering vector range, three instrument configurations were employed, defined by the sample-to-detector distance and neutron wavelength: 9 m/15–17.8 Å, 4 m/10–13.6 Å, and 2.5

m/2.5–6.4 Å. Covering the range $0.0023 < q < 0.75$ Å^{-1}, q is scattering vector define by $q = (4\pi/\lambda)\sin(\theta/2)$, where λ is the wavelength of the neutrons and θ is the scattering angle.

Data reduction was performed using the drtsans software package [35], accounting for detector sensitivity, background subtraction, and absolute scale calibration. Data analysis was performed using SasView software (version 6.1.1) [36]. A power-law model was initially applied to assess the general structural features of the samples. Subsequently, quantitative fitting was carried out using a core – shell ellipsoidal form factor model. Structural parameters obtained from transmission electron microscopy (TEM), including core dimensions and particle ellipsoid shape, were used as initial constraints in the fitting procedure, while shell-related parameters were refined during model optimization.

3. Results

3.1 Structural and morphological characterization of polymer-grafted silica nanoparticles

The successful stepwise synthesis and surface functionalization of the nanoparticles were confirmed by FTIR spectroscopy (Figure 1). The spectrum of SiO_2 (Figure 1a) exhibits the characteristic peaks at 1060 and 800 cm^{-1}, assigned to Si–O–Si (siloxane bonds) stretching vibrations, along with a shoulder at around 975 cm^{-1} corresponding to silanol group (– Si–OH). After surface modification, the spectrum of SiO_2/VSyl (Figure 1b) reveals the appearance of new, albeit weak, absorption bands. The peaks at 1604, 1621, and 3060 cm^{-1} correspond to the C=C and =C–H stretching vibrations, respectively. Additionally, the peak at 1409 cm^{-1} corresponds to the $=CH_2$ bending of the vinyl group, while the bands at 2860 and 2967 cm^{-1} are assigned to the C–H stretching of unreacted methoxy groups, confirming the successful anchoring of the silane coupling agent onto the silica surface.

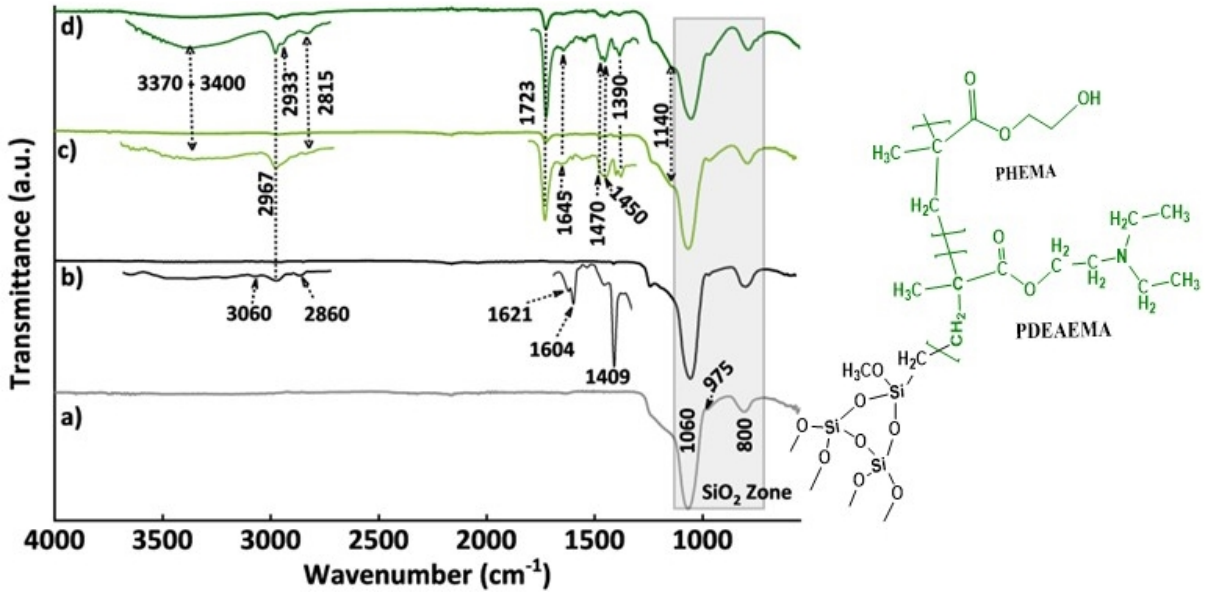

Figure 1. FTIR spectra of a) bare SiO_2; b) vinyl-modified silica (SiO_2/VSyl); and the core-shell hybrids c) **p1**$_{\text{DEAEMA-}co\text{-HEMA}}$ and d) **p2**$_{\text{DEAEMA-}co\text{-HEMA}}$. **Inset**: Schematic representation of the SiO_2 core grafted DEAEMA-*co*-HEMA polymeric shell.

Furthermore, the FTIR spectra of the hybrids p1 (**Figure 1c**) and p2 (**Figure 1d**) display new absorption bands characteristic of the DEAEMA-*co*-HEMA copolymer. These include a strong ester carbonyl (C=O) stretching vibration at 1723 cm^{-1} and a broad O – H stretching band associated with HEMA units in the 3370–3400 cm^{-1} region. The DEAEMA incorporation into the grafted copolymer is evidenced by bands at 2815 and 1450 cm^{-1}, assigned to aliphatic C–H stretching and scissoring vibrations, respectively. The band at 1470 cm^{-1} can be attributed to C–N related vibrational modes coupled with $–CH_2–$ deformations of the tertiary amine groups ($–NCH_2–$), consistent with poly(DEAEMA)-based systems [13, 37]. Moreover, the C–O stretch at 1140 cm^{-1}, together with the intense aliphatic C–H stretching vibrations in the 2933–2967 cm^{-1}, confirm the presence of the grafted polymer backbone and DEAEMA and HEMA side chains on the silica surface. Notably, the co-polymer shell bands (C=O, C–N, C–H, and O–H) show higher intensity in the p2 than in p1.

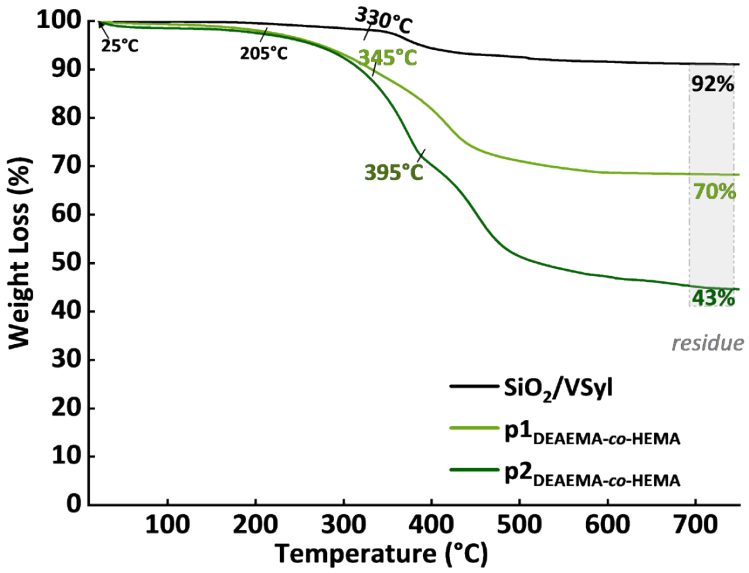

Figure 2. Thermogravimetric analysis (TGA) curves of SiO_2/VSyl, **p1**$_{DEAEMA\text{-}co\text{-}HEMA}$ and **p2**$_{DEAEMA\text{-}co\text{-}HEMA}$ systems. Residual masses at 750 °C were used to estimate polymer grafting contents after correcting for the contribution of the vinyl-silane layer.

Thermogravimetric analysis (TGA) was used to measure the amount of organic material grafted onto the silica nanoparticles (**Figure 2**). The vinyl-functionalized silica precursor (SiO_2/VSyl, black curve) exhibits high thermal stability, retaining approximately 92% of its initial mass at 750 °C. The sample displays two degradation steps, the initial weight loss of 2% corresponds to the desorption of physisorbed water molecules, and the second weight loss, which starts at 330 °C, is due to the degradation of the vinyl-silane grafted organic material. This indicates that the functionalization accounts for approximately 6% (DS = 0.233, see the Supplementary Material-SM2).

The p1 sample (light green curve) displays a gradual mass loss, resulting in a final residue of 70% at 750°C, whereas the p2 sample (dark green curve) exhibits a substantially larger mass loss, yielding a final residue of approximately 43% at 750°C. The thermograms of these core-shell systems reveal three distinct weight loss events at different temperature regions. The first is associated with the desorption of physisorbed water. The second event, starting at 205 °C, is due to degradation of the amine side groups from DEAEMA. The accelerated weight loss initiated at 345 and 395 °C for p1 and p2, respectively. This was attributed to the complete thermal degradation of the DEAEMA-*co*-HEMA shell.

The polymer grafting content was estimated using the residual mass of SiO_2/VSyl (92%) to correct for the contribution of the silane layer. The net polymer content is estimated to be 22% for p1 and 49% for p2. The higher polymer content in p2 is consistent with the stronger FTIR polymer bands and the thicker shell observed by TEM.

Transmission electron microscopy (TEM) was employed to characterize the morphology, size, and core–shell architecture of the synthesized nanoparticles (**Figure 3**). Representative TEM micrographs of the silica core (**Figure 3a**) reveal well-defined particles with predominantly ellipsoidal morphology and relatively smooth surfaces. A detailed quantitative morphological analysis of the silica cores is provided in supplementary material (**Figure SM1**).

For size analysis, particle dimensions were extracted from TEM images (100–150 kx) by measuring the equatorial radius (r_{eq}) of ~80 silica cores. The resulting size distribution (see **Figure SM1**) revealed an average equatorial diameter of 154 ± 22 nm, with particle sizes ranging from 110 to 206 nm. The relatively narrow size distribution corresponds to low geometric polydispersity (PDI = 0.15). Additionally, particle anisotropy was determined using the polar–to–equatorial radius ratio (r_{polar}/r_{eq}), calculated from high-magnification TEM images (see **Figure SM1b**). The calculated aspect ratios of 1.15–1.25 confirm the ellipsoidal morphology of the silica particles.

Consistent with the successful polymer grafting confirmed by FTIR and TGA, TEM images of the core-shell hybrids reveal a lower-electron-density outer region surrounding the silica cores, attributed to the grafted polymer layer. In the p1 sample (**Figure 3b**), the particles remain predominantly well dispersed, exhibiting a weak, relatively homogeneous low contrast shell. In contrast, the p2 sample **(Figure 3c**) displays a visibly thicker polymer region and a higher tendency toward aggregation, particularly at lower magnification (**Figure 1c**, left panel). This behavior suggests an increased polymer grafting content, which promotes interparticle interactions and modifies the effective particle surface.

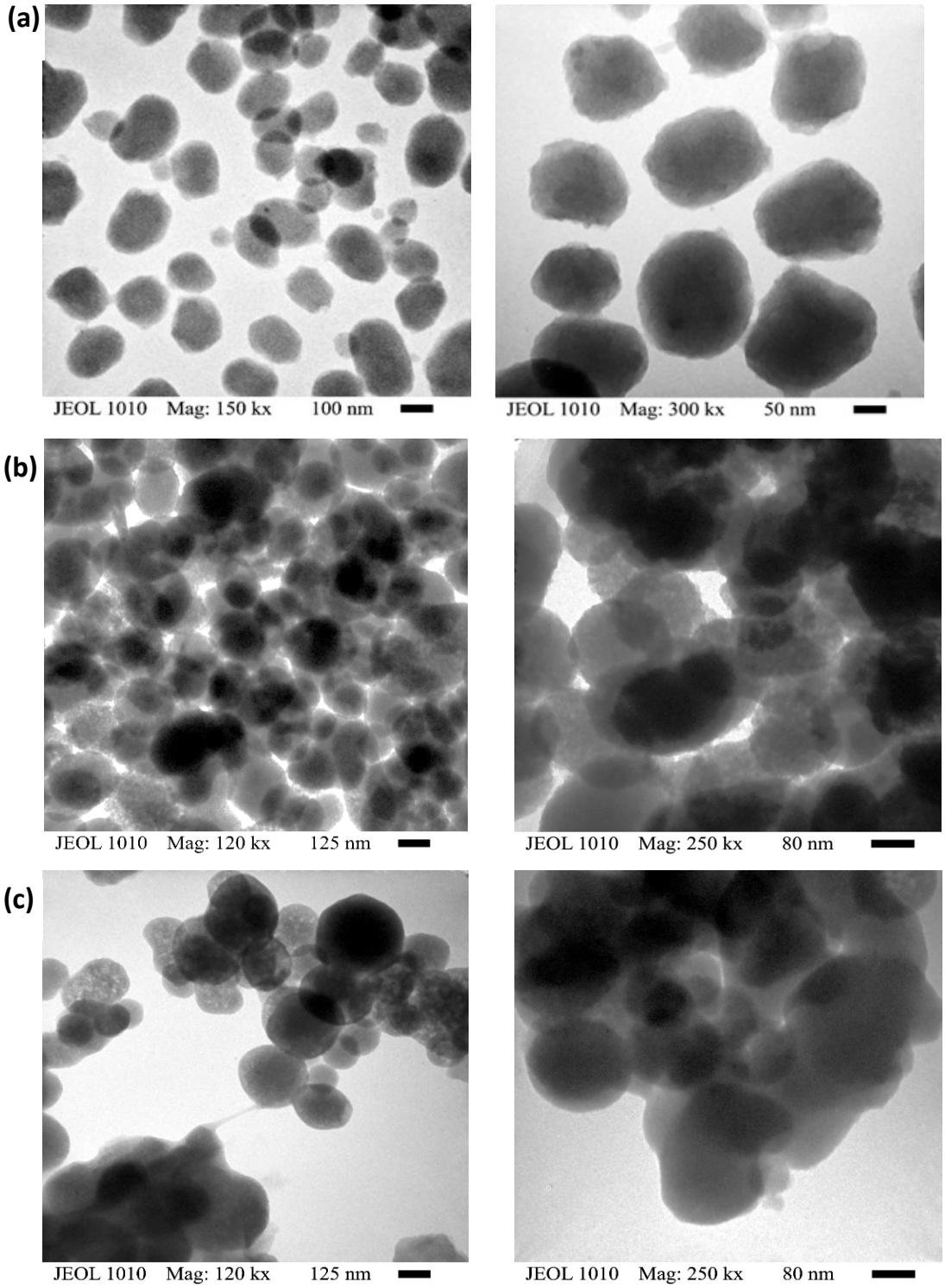

Figure 3. TEM micrographs of core-shell hybrid nanoparticles**.** (a) pristine ellipsoidal SiO_2 particles with a narrow size distribution, (b) **p1**$_{\text{DEAEMA-}co\text{-HEMA}}$ and (c) **p2**$_{\text{DEAEMA-}co\text{-HEMA}}$ hybrids maintain the SiO_2 core morphology and exhibit an external diffuse region attributed to the polymer shell, which promotes particle aggregation. Left panels: low-magnification; right panels: high-magnification showing surface details.

Table 2. Physicochemical and textural properties of silica core and $\mathbf{p_{DEAEMA\text{-}co\text{-}HEMA}}$ core-shell hybrids.

Sample	[a]Grafting %wt	[b]Atomic ratio N/Si	[b]DEAEMA		[b]HEMA		[c]S_{BET} $m^2\,g^{-1}$	[c]V_P $cm^3\,g^{-1}$	[c]D_P nm
			%mol	%wt	%mol	%wt			
SiO_2	n.d						1100	1.37	2.48
SiO_2/VSyl	6	n.d					965	1.12	2.12
$p1_{DEAEMA\text{-}co\text{-}HEMA}$	22	0.19	47.60	56.30	52.40	43.70	235	0.301	1.18
$p2_{DEAEMA\text{-}co\text{-}HEMA}$	49	0.47	69.60	76.50	30.40	23.50	110	0.138	1.01

[a]Determined by TGA. [b]Estimated from XPS using N 1s (DEAEMA) and oxygenated carbon component (HEMA) as tracers. [C]Determined by N_2 physisorption (BET method). V_P = pore volume; D_P = pore size

The textural properties of the bare silica (SiO_2), silane-modified silica (SiO_2/VSyl) and the $p_{DEAEMA\text{-}co\text{-}HEMA}$ hybrids were evaluated using N_2 adsorption–desorption analysis (**Table 2**). The SiO_2 demostrated a high BET surface area (S_{BET}) of 1100 $m^2\,g^{-1}$, large pore volume (V_p) of 1.37 $cm^3\,g^{-1}$, and a pore diameter of 2.48 nm, typical of well-developed mesoporous silica. Subsequent to polymer grafting, all textural parameter decreased significantly, due to the presence of the polymer shell. For the 22% grafted sample, the S_{BET} and V_p decreased to 235 $m^2\,g^{-1}$ and 0.301 $cm^3\,g^{-1}$, respectively. A more pronounced reduction occurred in the 49% grafted sample (110 $m^2\,g^{-1}$ and 0.138 $cm^3\,g^{-1}$). Accordingly, the average pore diameter decreased from 2.48 nm in the SiO_2 core to 1.18 nm (22% grafted) and 1.01 nm (49% grafted). This reduction in textural parameters is attributed to a pore filling and blockage of the mesoporous channels upon polymer grafting, especially in p2 due to the higher polymer content, aligning with TEM observations of a thicker polymer shell and aggregation for p2. Together, these results suggest that a increasing polymer content extensively modifies of both the external surface and the accessible porosity of the silica nanoparticles.

3.2 Surface chemical composition and bonding analysis

X-ray photoelectron spectroscopy was used to gain deeper insight into the surface chemical composition and to further confirm the successful grafting of the DEAEMA-*co*-HEMA shell. The elemental compositions and the results from the high-resolution C 1s deconvolution are summarized in **Table 3**, while the corresponding survey and high-resolution spectra are shown in **Figure 4**.

The survey spectra reveal a systematic change in the surface stoichiometry with each functionalization step. The SiO_2 and SiO_2/VSyl samples are dominated by silicon (Si 2p) and oxygen (O 1s) signals. After polymer grafting, a pronounced attenuation of the Si 2p signal is observed, decreasing from 26.37 at. % for SiO_2/VSyl to 13.61 and 8.78 at. % for p1 and p2, respectively. Concurrently, the carbon (C 1s) content increases significantly from 20.82 to 61.46 at. %, and nitrogen (N 1s), which is absent in the precursor materials, appear at 2.62 at. % for p1, increasing to 4.16 at. % for p2. This evolution is consistent with the formation of a polymer-rich surface layer that progressively shields the underlying silica core as the grafting density increases.

Further structural information is obtained from the deconvolution of the high-resolution C 1s spectra. For the SiO_2/VSyl sample, the spectrum is primarily composed of contributions from C–Si (283.33 eV) and C=C (284.16 eV) bonds, confirming the successful attachment of vinyl groups onto the silica surface.

In contrast, the hybrids p1 and p2 exhibit additional chemical environments characteristic of the DEAEMA and HEMA moieties. The component at ~286.1 eV is assigned to C–N bonds associated with the tertiary amine groups of DEAEMA, which are responsible for the pH-responsive behavior of the copolymer. The peak at 288.0 – 288.5 eV corresponds to ester carbonyl (C=O) groups present in both methacrylate units, while the contribution at 286.6 – 286.8 eV is attributed to C–OH bonds from the hydroxyl groups of the HEMA segments, contributing to the hydrophilic character of the shell. The presence and relative intensities of these components indicate that the characteristic functional groups of both monomers are preserved after radical polymerization and surface grafting.

Table 3. Surface chemical composition of the synthesized nanomaterials determined by XPS survey scans and high-resolution C 1s spectral deconvolution.

Sample	Elemental composition (at%)				C1s Deconvolution		
	Si 2p	O 1s	C 1s	N 1s	Assignment	B.E. (eV)	Comp. (%)
SiO_2	30.42	69.58	n.d.	n.d	n.d		
SiO_2/VSyl	26.37	52.81	20.82	n.d	C – Si	283.33	47.37
					C = C	284.16	37.73
					C – H	285.17	10.77
					C – O	286.50	4.14
p1$_{DEAEMA\text{-}co\text{-}HEMA}$	13.61	35.93	47.84	2.62	C – Si	283.96	23.16
					C – C	284.76	29.97
					C – H	285.44	17.19
					C – N	286.09	11.02
					C – OH	286.64	6.04
					C – O	287.67	3.73
					C = O	288.51	8.88
p2$_{DEAEMA\text{-}co\text{-}HEMA}$	8.78	25.60	61.46	4.16	C – Si	283.76	22.94
					C – C	284.50	30.75
					C – H	285.30	22.08
					C – N	286.11	8.48
					C – OH	286.80	2.95
					C – O	286.89	4.07
					C = O	288.00	8.74

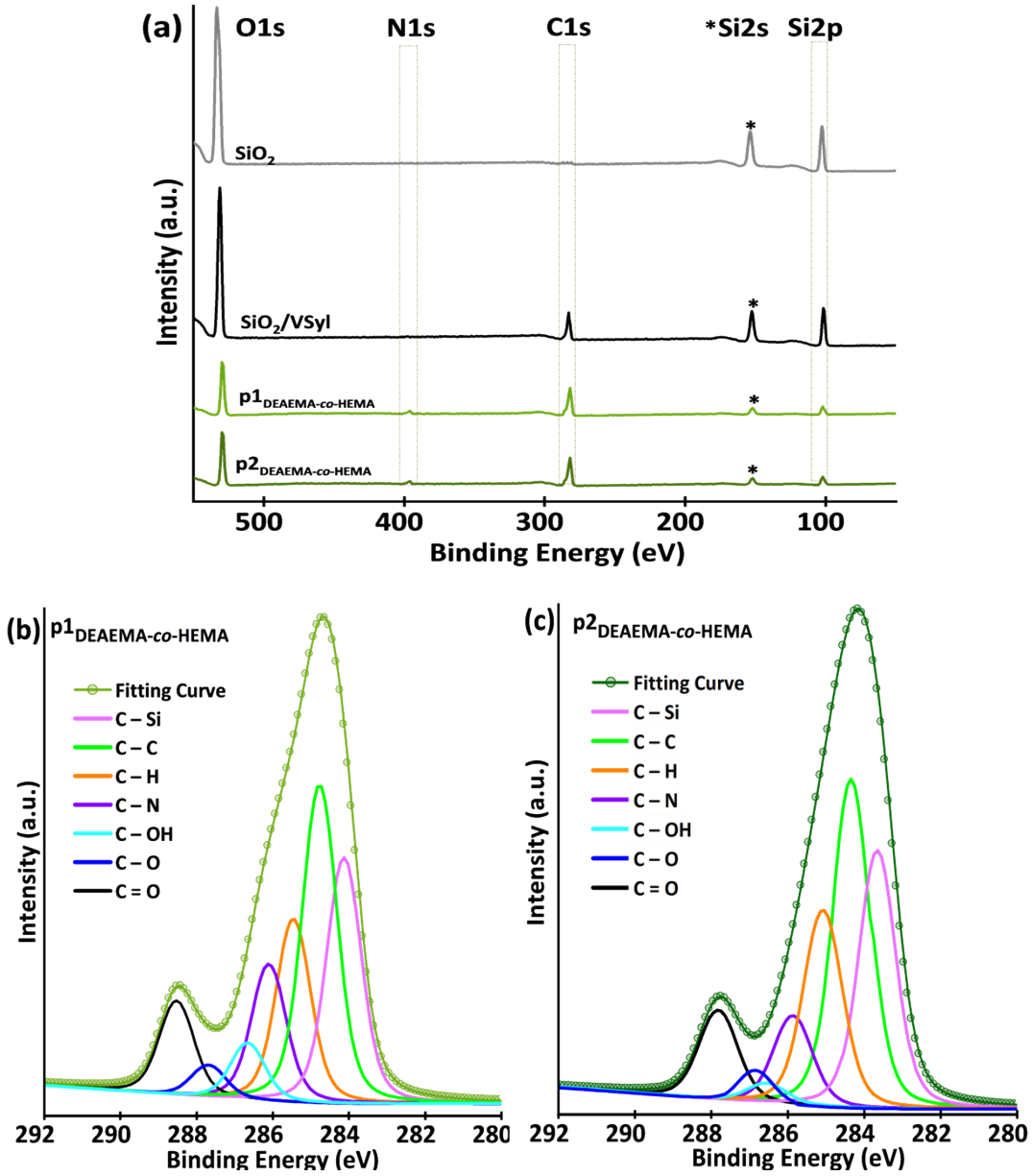

Figure 4. XPS analysis of the synthesized core-shell hybrid nanoparticles. (a) Survey spectra of core SiO_2 , SiO_2/VSyl, and the core-shell hybrids $p1_{DEAEMA\text{-}co\text{-}HEMA}$ and $p2_{DEAEMA\text{-}co\text{-}HEMA}$. High-resolution C 1s core-level spectra of the: (b) $p1_{DEAEMA\text{-}co\text{-}HEMA}$ and (c) $p2_{DEAEMA\text{-}co\text{-}HEMA}$, showing the curve fitting and deconvolution into specific chemical bonds.

The copolymer's relative surface composition, estimated from XPS elemental ratios, is summarized in Table 2. Nitrogen N 1s and oxygenated carbon served as elemental markers for DEAEMA and HEMA units, respectively. These semi-quantitative surface fractions reflect the XPS probing depth and are intended for comparative analysis rather than absolute bulk compositions.

The increasing N/Si atomic ratio from the p1 to the p2 reflects a higher surface content of DEAEMA units, in agreement with the larger polymer grafting amount determined by TGA. Accordingly, the

surface molar and mass fractions indicate a clear enrichment of DEAEMA in the p2 sample compared to p1, consistent with the stronger attenuation of the Si signal and the higher nitrogen content observed in the survey spectra.

3.3 Conformational analysis and core-shell architecture

Building on the surface composition and grafting content established by FTIR, TGA, and XPS. The pH-dependent surface charge behavior of the hybrid materials was evaluated via zeta potential measurements, as shown in Figure 5. For comparison, homopolymer-grafted references were included, SiO_2-pHEMA (24% grafted, prepared as previously reported [16] and SiO_2-pDEAEMA (35% grafted, prepared analogously using only DEAEMA). The SiO_2-pDEAEMA exhibits the highest positive surface charge at acidic pH (+35 mV at pH 2), which is characteristic of the protonation of tertiary amine groups [10]. In contrast, the copolymer-grafted systems, $p1_{DEAEMA\text{-}co\text{-}HEMA}$ and $p2_{DEAEMA\text{-}co\text{-}HEMA}$, display lower zeta potentials at the same pH (~ +18 mV). This reduction in positive charge occurs when PHEMA is introduced, and then this polymer protects the protonation of the am ino groups of PDEAEMA, which moderates the overall surface potential. As the DEAEMA:HEMA mass ratio was constant, i.e., the chemistry of the surface is the same in both samples, the zeta potential at pH 2 remains constant regardless of the thickness detected in TEM micrographs of TGA profiles.

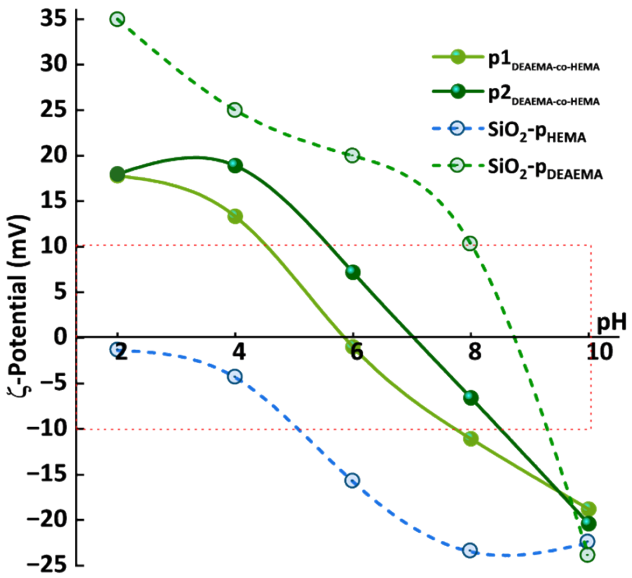

Figure 5. Zeta potential as a function of pH for the homopolymer-grafted silica (SiO_2-pHEMA 24% grafted and SiO_2-pDEAEMA 35% grafted) and core-shell systems ($p1_{DEAEMA\text{-}co\text{-}HEMA}$, $p2_{DEAEMA\text{-}co\text{-}HEMA}$). The red dotted area highlights the instability region where particles are prone to aggregation.

A key feature of the ζ-potential profiles is the systematic shift of the isoelectric point (IEP) among the samples, which can be rationalized in terms of the effective pK_a of the grafted polymer shell. The SiO_2–

pDEAEMA system remains positively charged up to pH ≈ 8.5, in agreement with the relatively pK_a reported for DEAEMA (~ 6.7)[9]. In contrast, the copolymer-grafted ($p_{DEAEMA\text{-}co\text{-}HEMA}$) nanoparticles cross the neutrality line at significantly lower pH values. The p1 sample reaches its IEP at pH ≈ 5.8, whereas p2, which contains a higher surface density of amine groups as evidenced by XPS (higher N/Si ratio), maintains a positive surface charge up to pH ≈ 6.8 (IEP).

This behavior indicates that the effective pK_a of the copolymer shell, as determined by potentiometric titration, increases with increasing DEAEMA content. Apparent pK_a values of 5.4 for p1 and 5.9 for p2 were obtained, reflecting the combined effects of copolymer composition, grafting content, and the local chemical environment imposed by the silica surface. The isoelectric point (IEP) variation reflects contributions from all ionizable groups (amines, hydroxyls and, silanols), whereas pK_a measures only amine protonation. The shift toward lower IEP values in the p1 and p2 systems compared to the DEAEMA homopolymer reflects the influence of the HEMA, which reduces amine basicity and promotes earlier charge neutralization.

At physiological and alkaline pH values (pH 8–10), all systems transition to negative values. At pH 10, p1 and p2 reach potentials of approximately –19 mV and –21 mV, respectively. This charge reversal is attributed to the deprotonation of hydroxyl-containing segments within the grafted shell and the adsorption of hydroxyl ions, in agreement with the negative ζ-potential values observed for the SiO_2-pHEMA reference sample in the same pH range (**Figure 5**).

According to the stability criteria [38] the region between +10 mV and –10 mV (red dotted area) indicates a zone of colloidal instability. However, the p2 sample exhibits a broader stability range in the acidic region compared to p1, which is consistent with its higher degree of functionalization observed in TGA, FTIR and XPS. This pH-responsive profile is particularly promising for anticancer drug delivery, as the charge reversal occurs precisely within the pH gradient between healthy tissue (~7.4) and the acidic environments of the tumor microenvironment (6.5–6.8) and intracellular endo/lysosomes (4.5–6.0), providing a potential triggered for targeted cargo release [11-13].

To move beyond surface characterization and elucidate the three-dimensional organization of the polymer shell in the hydrated state. Small-angle neutron scattering (SANS) measurements were performed at pH 2, where p1 and p2 exhibit a net positive surface charge (**Figure 5**), and the grafted polymer shell is highly hydrated and expanded. While TEM provides local, dry-state morphological information, the SANS profiles (**Figure 6**) enable bulk-averaged structural analysis in solution under controlled contrast conditions.

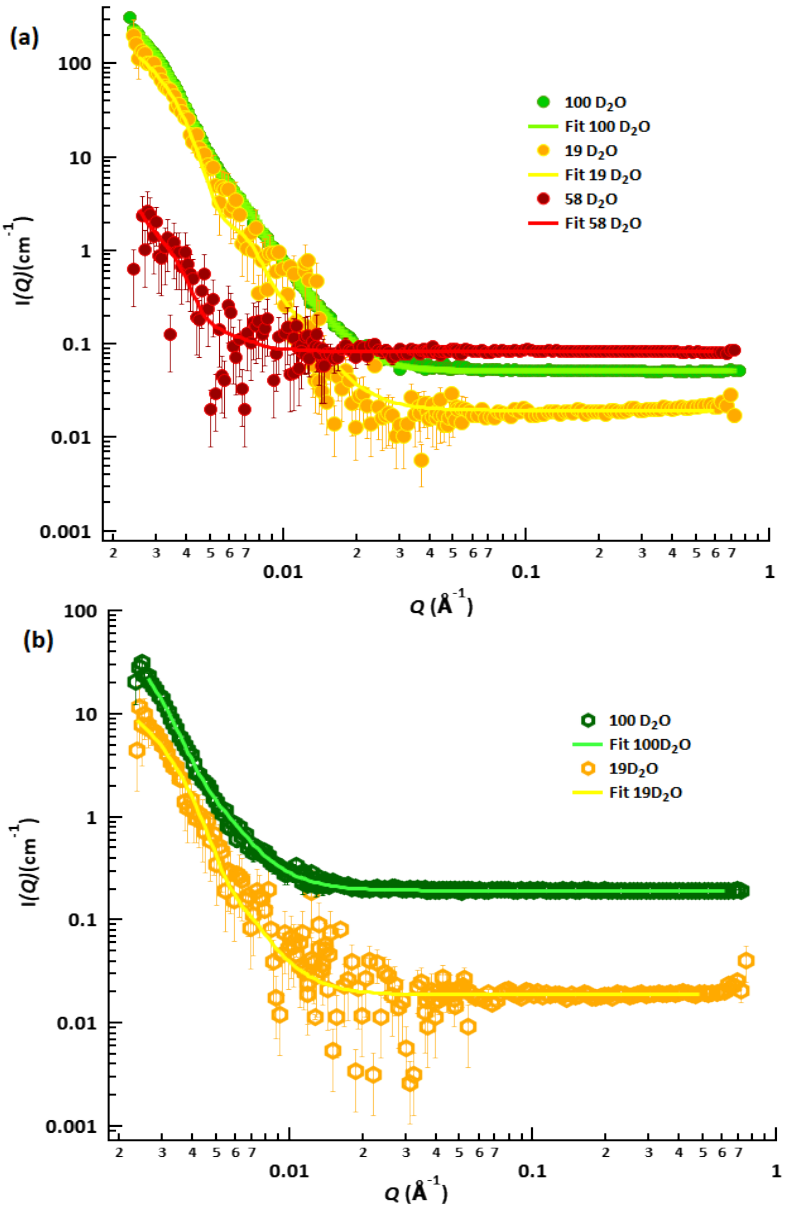

Figure 6. SANS patterns of DEAEMA-co-HEMA shell grafted mesoporous silica nanoparticles after background subtraction. (a) $p1_{DEAEMA\text{-}co\text{-}HEMA}$ at 100, 58 and 19% D_2O in PBS (pH 2) contrast settings and (b) $p2_{DEAEMA\text{-}co\text{-}HEMA}$ in 100 and 19 % D_2O contrast. Symbols represent experimental data whereas the solid lines correspond to the best global fits obtained using the core-shell ellipsoid model.

An shown in **Figure 6,** the scattering curves collected under different %D_2O solvent contrasts exhibit a pronounced decay of intensity at low-*q*, consistent with the presence of nanoscale core–shell particles in solution. Remarkably, at 58% D_2O, where solvent matches the silica core, the scattering intensity drops significantly, especially for p2. In this condition, the scattering intensity is mostly from the unmatched polymer shell, and it is significantly reduced compared to other D_2O/H_2O contrasts.

However, this condition increases statistical noise, especially in the low-*q* region. For this reason, the p2 curve of at 58% D_2O (**Figure SM2**) serves only as qualitative evidence of core contrast matching rather than serving quantitative purposes. Conversely, measurements in 100% D_2O exhibit the highest scattering intensity and signal-to-noise ratio for both samples. This clearly resolves both the silica core and polymer shell, providing optimal data for extracting structural parameters. Additionally, measurements at 19% D_2O, the theoretical contrast-match point of the shell (Table SM2), were included to isolate the core signal and probe contrast-dependent variations. Despite increased low-*q* noise, the data retain sufficient structural information to support comparative analysis and model consistency.

As a first model-independent assessment, the SANS data were analyzed using a power-law approach in the low- to intermediate-*q* regime (Table SM1), where interfacial scattering dominates, since the scattering intensity flattens into an incoherent background at high-*q*. For both p1 and p2 systems, the scattering exponent remains close to $n \approx 4$ under most contrast conditions, consistent with behavior from compact objects with relatively sharp interfaces. Notably, under the 58% D_2O contrast, where the silica core is close to contrast-matched, a slightly lower exponent ($n \approx 3.8$) is observed. This deviation indicates a more diffuse interfacial region and enhanced sensitivity to the hydrated polymer shell, supporting the presence of an extended grafted layer rather than a sharp core–solvent boundary.

Based on the contrast-dependent signal quality and the non-spherical core geometry observed by TEM (aspect ratio 1.2, equatorial radius 77 nm, polar radius 92.4 nm), the core–shell ellipsoidal model was fitted using constrained parameters across selected solvent contrasts (section **SM 3.2** and Tables **SM2-3**).

For p1, global fitting included 100%, 58%, and 19% D_2O datasets, whereas for p2, it included 100% and 19% D_2O only. Due to near-complete core contrast matching and low signal-to-noise ratio, the 58% D_2O data for p2 was excluded from quantitative modeling.

Representative scattering curves and model fits are shown in Figure 6, with the extracted structural parameters summarized in Table 4. This combined analysis highlights the contribution of SANS to the structural characterization of the copolymer-grafted silica nanoparticles. While TEM provides direct visualization of the silica core morphology in the dry state, yielding equatorial and polar core dimensions (R_eq_core = 77 nm and R_polar_core = 92.40 nm), it offers limited insight into the spatial organization of the polymer shell under hydrated conditions. Similarly, shell thicknesses estimated from TGA (~13 nm and ~34 nm for p1 and p2, respectively) reflect the relative grafted polymer mass fractions but assume a completely compact state, ignoring swelling and chain conformation effects in solution.

In contrast, SANS core–shell modeling reveals significantly larger effective shell dimensions in the hydrated state, with polar shell thicknesses of 55.86 nm and 71.36 nm, respectively. Responsive polymer-grafted silica systems are reported to form dense, nearly solvent-free collapsed layers near the core [39]. In contrast, this discrepancy demonstrates that the copolymer DEAEMA-*co*-HEMA shell adopts a massively hydrated and extended conformation in its native solution state, an effect unresolved by gravimetry and dry-state imaging techniques alone[40].

Table 4. Parameters of: (A) SiO_2 Core obtained from TEM analysis; (B) Shell thickness (***t***) based on TGA weight percentage; (C) SANS results from constrained core–shell model fitting and (D) Pair distribution (*P(r)*) model-independent size.

	Parameter (nm)		$p1_{DEAEMA\text{-}co\text{-}HEMA}$	$p2_{DEAEMA\text{-}co\text{-}HEMA}$
(A)	$R_{\_eq\_core}$		77.00 ± 11	
	$D_{\_eq\_core}$		154.00 ± 22	
	$X_{\_core}$		1.20 ± 0.05	
	$R_{\_polar\_core}$		92.40 ± 13.75	
	$D_{\_polar\_core}$		184.8 ± 27.5	
(B)	$t_{shellTGA}$		13.00 ± 2.19	34.00 ± 2.67
	$D_{\_eff}$		163.64 ± 17.56	163.64 ± 17.56
	$D_{Total\ TGA}$		176.64 ± 17.70	197.64 ± 17.75
(C)	$Thick_{shellSANS}$		145.36 ± 0.789	198.22 ± 5.72
	$X_{\_polar\_shell}$		0.384 ± 0.0068	0.360 ± 0.030
	$Thick_{\_polar}$		55.82 ± 1.06	71.36 ± 6.3
	$D_{Totaleq}$		299.36 ± 22.01	352.22 ± 22.73
	$D_{Totalpolar}$		240.62 ± 27.52	256.16 ± 28.21
(D)	R_{mean}	100	87.35 ± 3.42	89.56 ± 9.20
	D_2O (%)	19	80.05 ± 12.01	84.61 ± 29.20
	D_{max}	100	205.53 ± 8.03	216.23 ± 22.22
	D_2O (%)	19	174.02 ± 26.12	176.27 ± 60.81

(A) $R_{\_eq\_core}$ and $R_{\_polar\_core}$ equatorial and polar radius. (B) $D_{totalTGA}$: total diameter calculated using $D_{\_eff} + t_{shellTGA}$. Note that D = 2*R*.

Moreover, SANS provides direct access to shell anisotropy and overall particle dimensions in solution, highlighting the technique's capability to differentiate molecular-level structural heterogeneities at nanoparticle interfaces[41]. The total equatorial diameter increases from 299.36 nm (p1) to 352.22 nm (p2), confirming polymer layer growth with grafting content. This expansion exhibits pronounced thickness anisotropy, with equatorial (~145.36 and ~198.22 nm) and polar (55.82 and 71.36 nm) dimensions for p1 and p2, respectively. The decreasing shell anisotropy parameter further reflects a non-uniform, direction-dependent shell development in the hydrated state.

The observed shell heterogeneity and anisotropy can be rationalized in terms of the grafting-from polymerization strategy employed in this work. Unlike common models for polymer-grafted silica that assume an isotropic, spherically symmetric shell [17, 18, 20], or those that account for structural heterogeneity strictly through radial phase separation (e.g., concentric core-shell 'onion' models) [19], here the SANS analysis reveals an inherent direction-dependent development of the copolymer layer. This intrinsic structural feature is fundamentally different from the anisotropy reported in other silica nanocomposite systems, such as those described by Akcora et al. [42], where non-spherical structures (e.g., strings or sheets) emerge primarily from the collective self-assembly of multiple particles.

In contrast, the present results demonstrate that anisotropy is an intrinsic property of the individual DEAEMA-co-HEMA polymer shell architecture. In grafting-from systems, polymer chains grow directly from surface-anchored initiators, which inherently leads to spatial variations in chain length and local grafting density across the nanoparticle surface. As a result, the grafted polymer layer does not form a uniform shell but rather a heterogeneous and direction-dependent shell whose structure reflects both the polymerization mechanism and the local chemical environment at the silica surface [17, 43-46]. This architectural complexity distinctly contrasts with non-covalent polymer adsorption on silica, which typically yields either uniform surface coverage or induces inter-particle bridging and aggregation[47]. In this context, theoretical studies by Asai et. al [45] have demonstrated that, at a given grafting density, grafting-from mechanisms tend to produce less uniform surface coverage and greater anisotropy compared to grafting-to approaches, due to the absence of excluded-volume regulation during chain growth.

Furthermore, in p1 and p2 systems, these architectural complexities are exacerbated by the aqueous polymerization conditions. While the HEMA comonomer is highly water-soluble, the neutral DEAEMA monomer exhibits limited aqueous solubility. This difference in solvation likely drives local interfacial energetics that favor non-uniform, anisotropic polymer growth, a phenomenon similarly observed in seeded silica/polymer composites [43]. This interpretation is corroborated by the model-independent *P(r)* analyses (Figure SM3), showing systematically larger R_{mean} and D_{max} values for p2 compared to p1 across solvent contrasts, which significantly exceed dry-state estimates.

Finally, the anisotropic polymer shell resolved by SANS has important implications for molecular transport through mesoporous silica core [48]. The reduced polymer thickness in the polar regions implies locally less shielded pore entrances, leading to heterogeneous accessibility of the internal porous network. Under acidic conditions (pH 2), the grafted DEAEMA segments are protonated and highly solvated, suggesting that this non-uniform shell architecture may regulate diffusion without fully blocking pore access. Unlike responsive grafted systems that undergo large-scale macroscopic aggregation or abrupt phase separation in response to environmental stimuli [49], the anisotropic but colloidally stable structure of the p1 and p2 nanoparticles provides a subtle mechanism for transport control. Although drug loading and release were not investigated in this work, the SANS results provide a structural basis for understanding how grafting density and intrinsic anisotropic polymer distributions can influence molecular transport in mesoporous silica–polymer nanoparticles.

4. Conclusions

Mesoporous silica nanoparticles grafted with DEAEMA-*co*-HEMA copolymer shells (22% and 49% grafting) were successfully synthesized using a grafting-from approach in aqueous media. FTIR, TGA, TEM, and XPS analyses confirmed the progressive formation of a polymer-rich shell, with increasing polymer content and surface coverage from the $p1_{\text{DEAEMA-}co\text{-HEMA}}$ to the $p2_{\text{DEAEMA-}co\text{-HEMA}}$ hybrids.

While dry-state techniques via TEM and TGA revealed the core morphology and relative shell thickness, SANS provided insight into the three-dimensional organization of the polymer shell in the hydrated state. Contrast variation experiments combined with constrained core–shell ellipsoid modeling demonstrated that the grafted copolymer layer is highly solvated and significantly more extended than dry-state estimates suggest. Notably, SANS resolved pronounced shell anisotropy, with thinner polymer coverage in the polar regions than in the equatorial regions, particularly at higher grafting content.

This anisotropic shell architecture reflects the combined effects of the grafting-from polymerization mechanism and aqueous solvent conditions. Although drug loading kinetics were beyond the scope of this study, the SANS-resolved structure provides a structural framework for understanding how non-uniform polymer shell organization may influence pore accessibility and molecular transport in hybrid nanocarriers. Future studies will directly investigate how this anisotropic shell architecture influences pore accessibility and molecular transport relevant to controlled release in mesoporous silica systems. In parallel, acknowledging the lack of direct molecular-weight determination of the grafted chains, their molecular weight distribution and dispersity will be quantified to provide a more complete physicochemical description of the grafted polymer shell.

5. Acknowledgements

A portion of this research used resources at the Spallation Neutron Source, a DOE Office of Science User Facility operated by the Oak Ridge National Laboratory. The beam time was allocated to BL-6 (EQ-SANS) on proposal number IPTS-32504.1. Financial support for the research stay at ORNL was provided by the Academic Secretariat of CUCEI, University of Guadalajara. The authors also thank Armando Renteria (TEM) and José A. Rivera Mayorga (XPS, Project No. 270662-SECIHTI) from the Materials Laboratory (University of Guadalajara) for their technical support.

6. Author contributions

Lorena García-Uriostegui: Investigation, Formal analysis, Data curation, Conceptualization, Validation, Methodology, Visualization, Writing - original draft, Writing - review & editing, Funding acquisition, Project administration. **Shuo Qian**: Visualization, Validation, Resources, Formal analysis, Writing - review & editing, Project administration. **Gergely Nagy**: Methodology, Formal analysis, Visualization, Software, Writing - review & editing. **Gregorio Guadalupe Carbajal-Arizaga**: Visualization, Methodology. **H. Iván Meléndez-Ortiz:** Investigation, Methodology, Resources, Visualization.

7. References

[1] T.N. Aparna, R. Kumar, S.R. Ali, D.J. Patel, K. Julekha, T. Begum, J. Bala, P. Kumar, Silica Nanoparticles: A Promising Vehicle for Anti-Cancer Drugs Delivery, AAPS Pharm. Sci. Tech. , 26 (2025) 33, https://doi.org/10.1208/s12249-12024-02982-12249.

[2] M. Manzano, M. Vallet-Regí, Mesoporous Silica Nanoparticles in Biomedicine: Advances and Prospects, Adv. Mater., (2025) e12433, https://doi.org/12410.11002/adma.202512433.

[3] J. Yu, N. Dan, S.M. Eslami, X. Lu, State of the Art of Silica Nanoparticles: An Overview on Biodistribution and Preclinical Toxicity Studies, AAPS J. , 26 (2024) 35, https://doi.org/10.1208/s12248-12024-00906-w.

[4] Y. Liu, L. Si, Y. Jiang, S. Jiang, X. Zhang, S. Li, J. Chen, J. Hu, Design of pH-Responsive Nanomaterials Based on the Tumor Microenvironment, International journal of nanomedicine, 20 (2025) 705-721, https://doi.org/710.2147/IJN.S504629.

[5] S. Porrang, N. Rahemi, S. Davaran, M. Mahdavi, B. Hassanzadeh, Synthesis of temperature/pH dual-responsive mesoporous silica nanoparticles by surface modification and radical polymerization for anti-cancer drug delivery, Colloids Surf. A Physicochem. Eng. Asp. , 623 (2021) 126719, https://doi.org/126710.121016/j.colsurfa.122021.126719.

[6] L.H.K. Alfhaid, Recent advance in functionalized mesoporous silica nanoparticles with stimuli-responsive polymer brush for controlled drug delivery, Soft Mater., 20 (2022) 364-378, https://doi.org/310.1080/1539445X.1532022.2028831.

[7] M.d.l.Á. Cabrera Molina, B. Ivanoff, M.A. Lago Huvelle, G.J.A.A. Soler Illia, C.B. Contreras, Temperature and pH-Responsive Nanocarrier for Paclitaxel Controlled Release Based on P(NIPAM-co-HEMA)-Modified Silica Microgel, ACS Appl. Polym., 7 (2025) 8396-8410, https://doi.org/8310.1021/acsapm.8395c00648.

[8] E. Beňová, V. Hornebecq, V. Zeleňák, V. Huntošová, M. Almáši, M. Máčajová, D. Bergé-Lefranc, pH-responsive mesoporous silica drug delivery system, its biocompatibility and co-adsorption/co-release of 5-Fluorouracil and Naproxen, Appl. Surf. Sci., 561 (2021) 150011, https://doi.org/150010.151016/j.apsusc.152021.150011.

[9] L. Salminen, E. Karjalainen, V. Aseyev, H. Tenhu, Phase Separation of Aqueous Poly(diisopropylaminoethyl methacrylate) upon Heating, Langmuir, 38 (2022) 5135-5148, https://doi.org/5110.1021/acs.langmuir.5131c02224.

[10] K.M. Alotaibi, A.A. Almethen, A.M. Beagan, L.H. Alfhaid, M. Ahamed, A.M. El-Toni, A.M. Alswieleh, Poly(oligo(ethylene glycol) methyl ether methacrylate) Capped pH-Responsive Poly(2-(diethylamino)ethyl methacrylate) Brushes Grafted on Mesoporous Silica Nanoparticles as Nanocarrier, Polymers, 13 (2021) 823, https://doi.org/810.3390/polym13050823.

[11] H.-L. Su, L. Xu, X.-J. Hu, F.-F. Chen, G. Li, Z.-K. Yang, L.-P. Wang, H.-L. Li, Polymer grafted mesoporous SBA-15 material synthesized via metal-free ATRP as pH-sensitive drug carrier for quercetin, Eur. Polym. J., 148 (2021) 110354, https://doi.org/110310.111016/j.eurpolymj.112021.110354.

[12] T. Marcelino, M.A.R. Docampo, X. Qian, C. Ade, E. Brodszkij, M. Ceccato, M. Foss, M. Dulchavsky, J.C. Bardwell, B. Städler, Surfaces Coated with Polymer Brushes Work as Carriers for Histidine Ammonia Lyase, Macromol. Biosci., 23 (2023) 2200528, https://doi.org/2200510.2201002/mabi.202200528.

[13] J.L. Sanchez-Orozco, L.A. Garcia-Cerda, B. Puente-Urbina, H.I. Melendez-Ortiz, Poly (N-vinylcaprolactam-co-2-(diethylamino) ethylmethacrylate) coated Fe3O4@ SiO2 core-shell magnetic nanoparticles for controlled doxorubicin delivery, J. Drug Deliv. Sci. Technol., 81 (2023) 104253, https://doi.org/104210.101016/j.jddst.102023.104253.

[14] J.-T. Sun, C.-Y. Hong, C.-Y. Pan, Fabrication of PDEAEMA-coated mesoporous silica nanoparticles and pH-responsive controlled release, J. Phys. Chem. C, 114 (2010) 12481-12486, https://doi.org/12410.11021/jp103982a

[15] A. Alfawaz, K. Alzahrani, A. Niazy, H. Alghamadi, R. Lambarte, A. Beagan, L. Alfhaid, K. Alotaibi, A. Alswieleh, Smart Nanocarrier Based on Poly(oligo(ethylene glycol) methyl ether acrylate) Terminated pH-Responsive Polymer Brushes Grafted Mesoporous Silica Nanoparticles, Appl. Sci., 12 (2022) 3688, https://www.mdpi.com/2076-3417/3612/3687/3688.

[16] L. García-Uriostegui, H.I. Meléndez-Ortíz, T. Camacho-Villegas, P. Lugo-Fabres, G. Toriz, Physics, Synthesis and characterization of mesoporous silica-g-poly (hydroxyethylmethacrylate) nanohybrid particles as a drug delivery system, Mater. Chem., 283 (2022) 126048, https://doi.org/126010.121016/j.matchemphys.122022.126048

[17] R.W.N. Nugroho, K. Odelius, A. Höglund, A.-C. Albertsson, Nondestructive Covalent “Grafting-from” of Poly(lactide) Particles of Different Geometries, ACS Appl. Mater. Interfaces, 4 (2012) 2978-2984, https://doi.org/2910.1021/am3003507.

[18] M. Sokolowski, C. Bartsch, V.J. Spiering, S. Prévost, M.-S. Appavou, R. Schweins, M. Gradzielski, Preparation of Polymer Brush Grafted Anionic or Cationic Silica Nanoparticles: Systematic Variation of the Polymer Shell, Macromolecules, 51 (2018) 6936-6948, https://doi.org/6910.1021/acs.macromol.6938b01019.

[19] B.A. Humphreys, S.W. Prescott, T.J. Murdoch, A. Nelson, E.P. Gilbert, G.B. Webber, E.J. Wanless, Influence of molecular weight on PNIPAM brush modified colloidal silica particles, Soft. Matter., 15 (2019) 55-64, https://doi.org/10.1039/C1038SM01824C.

[20] M.A. Haque, T.G. Feric, S.T. Hamilton, A.-H.A. Park, M.D. Dadmun, Structure and Dispersion of Free and Grafted Polymer in Nanoparticle Organic Hybrid Materials-Based Solutions by Small-Angle Neutron Scattering, J. Phys. Chem. C, 125 (2021) 5327-5334, https://doi.org/5310.1021/acs.jpcc.5320c10790.

[21] W. Wang, R. Chen, H. Sun, M. Fei, Z. Wang, Incorporation of hydrogen bonding interactions with physical crosslinking to endow applicable mechanical property for microcrystalline cellulose-graft

bottlebrush copolymer elastomers, J. Colloid Interface Sci., 709 (2026) 139965, https://doi.org/139910.131016/j.jcis.132026.139965.

[22] W. Wang, J. Zhang, Z. Wang, X. Wang, Bottlebrush Cell-g-PBA-b-PMMA Copolymer Elastomers with Disentangled Short Side Chains To Possess Applicable Mechanical Properties, Macromolecules, 59 (2026) 925-938, https://doi.org/910.1021/acs.macromol.1025c02821.

[23] N. Mukherjee, A. Das, M. Dhara, T. Jana, Surface initiated RAFT polymerization to synthesize N-heterocyclic block copolymer grafted silica nanofillers for improving PEM properties, Polymer, 236 (2021) 124315, https://doi.org/124310.121016/j.polymer.122021.124315

[24] S. Rudra, M. Dhara, M. Chakraborty, T. Jana, Fluorinated Polymer Brush-Grafted Silica Nanoparticles: Robust and Durable Self-Cleaning Coating Materials, ACS Appl. Polym. Mater., 5 (2023) 7443-7457, https://doi.org/7410.1021/acsapm.7443c01312

[25] M. Dhara, S. Rudra, N. Mukherjee, T. Jana, Hollow polymer nanocapsules with a ferrocenyl copolymer shell, Polym. Chem., 12 (2021) 3976-3991, https://doi.org/3910.1039/D3971PY00590A.

[26] S. Rudra, S. Mondal, M. Chakraborty, M.J. Swamy, T. Jana, Galactose Glycopolymer-Grafted Silica Nanoparticles: Synthesis and Binding Studies with Lectin, ACS Appl. Bio Mater., 7 (2024) 5689-5701, https://doi.org/5610.1021/acsabm.5684c00759.

[27] E.D.H. Mansfield, Y. Pandya, E.A. Mun, S.E. Rogers, I. Abutbul-Ionita, D. Danino, A.C. Williams, V.V. Khutoryanskiy, Structure and characterisation of hydroxyethylcellulose–silica nanoparticles, RSC Adv. , 8 (2018) 6471-6478, http://dx.doi.org/6410.1039/C6477RA08716K.

[28] W. Yang, J. Lu, E.P. Gilbert, R. Knott, L. He, W. Cheng, Probing Soft Corona Structures of DNA-Capped Nanoparticles by Small Angle Neutron Scattering, J. Phys. Chem. C, 119 (2015) 18773-18778, https://doi.org/18710.11021/acs.jpcc.18775b04494

[29] V. Candela-Noguera, P. Amorós, E. Aznar, M.D. Marcos, R. Martínez-Máñez, Systematic study of the implications of calcination and solvent extraction of the surfactant in MCM-41-type mesoporous silica nanoparticles, Microporous and Mesoporous Mater., 373 (2024) 113119, https://doi.org/113110.111016/j.micromeso.112024.113119.

[30] Q. Cai, Z.-S. Luo, W.-Q. Pang, Y.-W. Fan, X.-H. Chen, F.-Z. Cui, Dilute Solution Routes to Various Controllable Morphologies of MCM-41 Silica with a Basic Medium, Chem. Mater., 13 (2001) 258-263, https://doi.org/210.1021/cm990661z.

[31] B.T. Cheesman, A.J.G. Neilson, J.D. Willott, G.B. Webber, S. Edmondson, E.J. Wanless, Effect of Colloidal Substrate Curvature on pH-Responsive Polyelectrolyte Brush Growth, Langmuir, 29 (2013) 6131-6140, https://doi.org/6110.1021/la4004092

[32] C.T. Rueden, J. Schindelin, M.C. Hiner, B.E. DeZonia, A.E. Walter, E.T. Arena, K.W. Eliceiri, ImageJ2: ImageJ for the next generation of scientific image data, BMC bioinformatics, 18 (2017) 529, https://doi.org/510.1186/s12859-12017-11934-z.

[33] A. Herrera-Gomez, M. Bravo-Sanchez, O. Ceballos-Sanchez, M. Vazquez-Lepe, Practical methods for background subtraction in photoemission spectra, Surf. Interface Anal., 46 (2014) 897-905, https://doi.org/810.1002/sia.5453.

[34] W.T. Heller, M. Cuneo, L. Debeer-Schmitt, C. Do, L. He, L. Heroux, K. Littrell, S.V. Pingali, S. Qian, C. Stanley, V.S. Urban, B. Wu, W. Bras, The suite of small-angle neutron scattering instruments at Oak Ridge National Laboratory, J. Appl. Cryst., 51 (2018) 242-248, https://doi.org/210.1107/S1600576718001231

[35] W.T. Heller, J. Hetrick, J. Bilheux, J.M.B. Calvo, W.-R. Chen, L. DeBeer-Schmitt, C. Do, M. Doucet, M.R. Fitzsimmons, W.F. Godoy, G.E. Granroth, S. Hahn, L. He, F. Islam, J. Lin, K.C. Littrell, M. McDonnell, J. McGaha, P.F. Peterson, S.V. Pingali, S. Qian, A.T. Savici, Y. Shang, C.B. Stanley, V.S. Urban, R.E. Whitfield, C. Zhang, W. Zhou, J.J. Billings, M.J. Cuneo, R.M.F. Leal, T. Wang, B. Wu, drtsans: The data reduction toolkit for small-angle neutron scattering at Oak Ridge National Laboratory, SoftwareX, 19 (2022) 101101, https://doi.org/101110.101016/j.softx.102022.101101

[36] D.M. et al., SasView Version 6.1.1, 10.5281/zenodo.17237394.

[37] E. Tang, K. Du, X. Feng, M. Yuan, S. Liu, D. Zhao, Controlled synthesis of cellulose-graft-poly[2-(diethylamino)-ethyl methacrylate] by ATRP in ionic liquid [AMIM]Cl and its pH-responsive property, Eur. Polym. J. , 66 (2015) 228-235, https://doi.org/210.1016/j.eurpolymj.2015.1001.1041.

[38] Z. Németh, I. Csóka, R. Semnani Jazani, B. Sipos, H. Haspel, G. Kozma, Z. Kónya, D.G. Dobó, Quality by Design-Driven Zeta Potential Optimisation Study of Liposomes with Charge Imparting Membrane Additives, Pharmaceutics, 14 (2022) 1798, https://www.mdpi.com/1999-4923/1714/1799/1798.

[39] J.R.S. Martin, I. Bihannic, C. Santos, J.P.S. Farinha, B. Demé, F.A.M. Leermakers, J.P. Pinheiro, E. Rotureau, J.F.L. Duval, Structure of Multiresponsive Brush-Decorated Nanoparticles: A Combined Electrokinetic, DLS, and SANS Study, Langmuir, 31 (2015) 4779-4790, https://doi.org/4710.1021/acs.langmuir.4775b00530.

[40] Y. Wei, Y. Xu, A. Faraone, M.J.A. Hore, Local Structure and Relaxation Dynamics in the Brush of Polymer-Grafted Silica Nanoparticles, ACS Macro Lett., 7 (2018) 699-704, https://doi.org/610.1021/acsmacrolett.1028b00223.

[41] Y. Wu, X. Liu, A. Radulescu, L. Porcar, A. Krause-Heuer, H. Jiang, H. Yang, Y. Ke, T. Darwish, Z. Luo, Small-angle neutron scattering differentiates molecular-level structural models of nanoparticle interfaces, Nanoscale, 17 (2025) 3798-3808, https://doi.org/3710.1039/D3794NR04365K.

[42] P. Akcora, H. Liu, S.K. Kumar, J. Moll, Y. Li, B.C. Benicewicz, L.S. Schadler, D. Acehan, A.Z. Panagiotopoulos, V. Pryamitsyn, V. Ganesan, J. Ilavsky, P. Thiyagarajan, R.H. Colby, J.F. Douglas, Anisotropic self-assembly of spherical polymer-grafted nanoparticles, Nature Mater., 8 (2009) 354-359, https://doi.org/310.1038/nmat2404.

[43] Z. Zhang, H. Shao, X. Zhou, L. Zhao, H. Liu, X. Ji, H. Liu, Controllable synthesis of anisotropic silica/polymer composite particles via seeded dispersion polymerization, Mater. Chem. Phys., 195 (2017) 105-113, https://doi.org/110.1016/j.matchemphys.2017.1004.1024.

[44] X. Ji, M. Wang, X. Ge, H. Liu, Synthesis of Anisotropic Polymer/Inorganic Particles via Asymmetric Swelling–Dissolving Process, Langmuir, 29 (2013) 1010-1016, https://doi.org/1010.1021/la304806d.

[45] M. Asai, D. Zhao, S.K. Kumar, Role of Grafting Mechanism on the Polymer Coverage and Self-Assembly of Hairy Nanoparticles, ACS Nano, 11 (2017) 7028-7035, https://doi.org/7010.1021/acsnano.7027b02657.

[46] M.A. Haque, T.G. Feric, S.T. Hamilton, A.-H.A. Park, M.D. Dadmun, Insights into the Assembly and Conformation of Nanoparticle Organic Hybrid Materials (NOHMs) in Solution with Varying Grafting Type, ACS Appl. Polym. Mater., 6 (2024) 3354-3363. https://doi.org/3310.1021/acsapm.3353c03219.

[47] R. Joksimovic, S. Prévost, R. Schweins, M.S. Appavou, M. Gradzielski, Interactions of silica nanoparticles with poly(ethylene oxide) and poly(acrylic acid): Effect of the polymer molecular weight and of the surface charge, J. Colloid Interface Sci., 394 (2013) 85-93, https://doi.org/10.1016/j.jcis.2012.1011.1073.

[48] X. Zhang, C. Gao, M. Liu, Y. Huang, X. Yu, E. Ding, Synthesis and characterization of asymmetric polymer/inorganic nanocomposites with pH/temperature sensitivity, Appl. Surf. Sci., 264 (2013) 636-643, https://doi.org/610.1016/j.apsusc.2012.1010.1084.

[49] E.D.H. Mansfield, S.K. Filippov, V.R. de la Rosa, M.T. Cook, I. Grillo, R. Hoogenboom, A.C. Williams, V.V. Khutoryanskiy, Understanding the temperature induced aggregation of silica nanoparticles decorated with temperature-responsive polymers: Can a small step in the chemical structure make a giant leap for a phase transition?, J. Colloid Interface Sci., 590 (2021) 249-259, https://doi.org/210.1016/j.jcis.2021.1001.1044.